Solid Earth Discuss., 6, 191–228, 2014
www.solid-earth-discuss.net/6/191/2014/
doi:10.5194/sed-6-191-2014

Solid Earth
Discussions
Open Access

Future Antarctic bed topography and its implications for ice sheet dynamics

S. Adhikari[1,2], E. Ivins[1], E. Larour[1], H. Seroussi[1], M. Morlighem[3], and S. Nowicki[4]

[1]Jet Propulsion Laboratory, California Institute of Technology, 4800 Oak Grove Dr., Pasadena, CA 91109, USA
[2]Division of Geological and Planetary Sciences, California Institute of Technology, 1200 E. California Blvd., Pasadena, CA 91125, USA
[3]Department of Earth System Science, University of California – Irvine, 3200 Croul Hall, Irvine, CA 92697, USA
[4]Code 615, NASA Goddard Space Flight Center, Greenbelt, Maryland, USA

Received: 24 December 2013 – Accepted: 6 January 2014 – Published: 17 January 2014

Correspondence to: S. Adhikari (surendra.adhikari@jpl.nasa.gov)

Published by Copernicus Publications on behalf of the European Geosciences Union.

Abstract

The Antarctic bedrock is evolving as the solid Earth responds to the past and ongoing evolution of the ice sheet. A recently improved ice loading history suggests that the Antarctic Ice Sheet (AIS) is generally losing its mass since the last glacial maximum (LGM). In a sustained warming climate, the AIS is predicted to retreat at a greater pace primarily via melting beneath the ice shelves. We employ the glacial isostatic adjustment (GIA) capability of the Ice Sheet System Model (ISSM) to combine these past and future ice loadings and provide the new solid Earth computations for the AIS. We find that the past loading is relatively less important than future loading on the evolution of the future bed topography. Our computations predict that the West Antarctic Ice Sheet (WAIS) may uplift by a few meters and a few tens of meters at years 2100 and 2500 AD, respectively, and that the East Antarctic Ice Sheet (EAIS) is likely to remain unchanged or subside minimally except around the Amery Ice Shelf. The Amundsen Sea Sector in particular is predicted to rise at the greatest rate; one hundred years of ice evolution in this region, for example, predicts that the coastline of Pine Island Bay approaches roughly 45 mm yr^{-1} in viscoelastic vertical motion. Of particular importance, we systematically demonstrate that the effect of a pervasive and large GIA uplift in the WAIS is associated with the flattening of reverse bed, reduction of local sea depth, and thus the extension of grounding line (GL) towards the continental shelf. Using the 3-D higher-order ice flow capability of ISSM, such a migration of GL is shown to inhibit the ice flow. This negative feedback between the ice sheet and the solid Earth may promote the stability to marine portions of the ice sheet in future.

1 Introduction

Projecting the evolution of the AIS into the next few centuries relies on simulating a complex and non-linear coupled Earth system. A recent survey of experts by Bamber and Aspinall (2013) reveals that projections for AIS contribution to rate of sea level rise

at the year 2100 AD are generally rather moderate ($\sim 1.7\,\mathrm{mm\,yr^{-1}}$) and that the upper end of the spectrum of projections would be about 7 times this value, mainly owing to intensification of the dynamics of the WAIS. However, projections beyond 2100 AD are much more uncertain (Bindschadler et al., 2013) and are mainly limited by the poor knowledge of physics involved in the GL migration and ice shelf melting (e.g., Vaughan and Arthern, 2007; Walker et al., 2013). Furthermore, there is strong evidence that over the past four million years, during times of increased global atmospheric temperatures by 2–3 °C, the marine WAIS collapsed, and possibly some portions of the larger EAIS as well (Naish et al., 2009; Raymo et al., 2011; Cook et al., 2013).

If we are to improve our capabilities to assess the risk of the catastrophic consequences of partial collapse of AIS marine based ice currently locked to the Antarctic continent, steps must be taken to fully assess the role of solid Earth deformation over tens to thousands of years, during which time gravitational viscoelastic flow of the underlying mantle may act to change the stability of the AIS. Past assessments have been that isostatic uplift following the ice sheet retreat promoted stability of the WAIS near the end of the last deglaciation during the mid-Holocene (Thomas, 1976). More recently, the promotion of stability by GIA rebound has been shown with increasingly more sophisticated computations (Gomez et al., 2010, 2013). It is also now recognized that past AIS recession and ice flow direction are plausibly explained by strong interaction of ice loading with the solid Earth (Siegert et al., 2013). It is this ice-sheet/solid-Earth (IS/SE) interaction that we now explore in this paper for the AIS as a whole using the 2-D (plan-form) GIA (Ivins and James, 1999) and 3-D thermomechanical ice flow (Pattyn, 2003) capabilities of ISSM (Larour et al., 2012b).

1.1 IS/SE feedback: GL migration

Perhaps, the most important IS/SE feedback is associated with the GL migration (e.g., Lingle and Clark, 1985). For equilibrium sea level, any change in vertical bedrock elevation also changes the local sea depth. This perturbs buoyant forces in the regional

ocean water and may promote the migration of the GL. Uplift of the seabed occurs, for example, in response to thinning of the inland ice sheet, and it causes local sea depth to decrease. If the GL is in initial equilibrium but sea depth decreases due to bed uplift, the GL tends to advance towards the continental shelf (e.g., Weertman, 1974; Schoof, 2007). The conceptual illustration of this negative feedback is shown in Fig. 1a. Lingle and Clark (1985) explored the effect of GIA-related seabed uplift on GL migration for Ice Stream E, now known as MacAyeal Ice Stream, in the WAIS. The modeled GIA uplift, caused by thinning of the ice stream catchment area, delays the onset of GL retreat, thus reducing the rate of retreat during Holocene sea level rise. Notably, it was argued that the regional advance of Ross Sea GL may have occurred over the past three millennia. The gravitational attraction effects on local sea level developed later by Gomez et al. (2010) acts to amplify this negative feedback during ice sheet retreat, since the diminished mass behind the GL has less mutual gravitational attraction with adjacent sea water, thus causing local sea level to drop.

The pace and magnitude of GL migration are also dictated by the bedrock slope. If sea depth decreases (due to bed uplift and sea level drop associated with the thinning of inland ice) at the initially equilibrium GL on a reverse bed, for example, the GL tends to advance further on a relatively flat bed. It is therefore that the GLs associated with the Ross and Ronne Ice Shelves in the WAIS that have a relatively flat reverse bed are very sensitive (Conway et al., 1999). Capturing the dynamics of such sensitive GLs demands the proper understanding of interactions among the ice, the ocean and the solid Earth, and is indeed the key for successful modeling of the WAIS (e.g., Vaughan and Arthern, 2007; Katz and Worster, 2010).

1.2 Additional IS/SE feedbacks

There are other important feedback mechanisms that the solid Earth deformation provides to ice sheet. The GIA uplift can be important in providing basal resistance to ice flow and buttressing the ice sheet by raising bedrock pinning points (e.g. Favier et al., 2012; Siegert et al., 2013). This is easily conceived from Fig. 1b. The GIA-induced

changes in surface elevation and regional slope of the ice sheet may affect the gravitational driving stress, as well as some processes at the ice/atmosphere interface (e.g., surface mass balance). These perturb the momentum balance and affect the englacial velocity field (e.g., Cuffey and Paterson, 2010; Winkelmann et al., 2012), which in turn may impact on ice thermodynamics via changes in strain heating. Spatially varying bed uplifts also affect the hydraulic potential field and hence the subglacial hydrology and the sliding rate of ice sheet. There is additionally the complication of bulge migration, a broad scale phenomenon involving bending of the elastic lithosphere and mantle lateral flow. Due to the lateral motion of this topographic bulge, local crustal motions (and slopes) may change sign during GIA (e.g., Fjeldskaar, 1994).

These mechanisms are extremely difficult to isolate and quantify, and it is therefore not obvious whether (and in what circumstances) each of these acts to accelerate or inhibit the ice flow. As long as the thermomechanical ice sheet model and other companion models (e.g., surface mass balance model and hydrological model) are dynamically coupled with a comprehensive solid Earth model, however, most of these feedbacks are intrinsically taken into account.

1.3 New solid Earth computations

For large timescale (millennia) simulations, most of the ice sheet models (e.g., Pollard and DeConto, 2009; Hughes et al., 2011) capture the solid Earth physics of varying degrees of complexity (cf. Le Meur and Huybrechts, 1996). With the exception of the recent work of Gomez et al. (2013), none of these studies provides the explicit assessment of effects of GIA uplift on several aspects of ice sheet dynamics (e.g., GL migration and gravitational driving stress). Le Meur and Huybrechts (2001) explicitly pointed out the need for the more complete coupling that could be found in the wavelength-dependent relaxation spectra of viscoelastic solid Earth models. In this paper, we quantify two distinct IS/SE feedback mechanisms applied to the AIS on centennial timescales using multiple wavelength dependent decay spectra. Assuming the equilibrium sea level, we first evaluate how the future bed uplift (governed by the past

and future evolution of AIS; cf. Sect. 2) controls the GL migration. Second, we assess the role of bed uplift on the gravitational driving stress. The overall influence of solid Earth deformation (via changes in GL and driving stress) on the ice surface velocities is also quantified. These assessments, based on reliable models and data, help to understand whether the GIA effects are significant in controlling the future evolution of AIS on centennial timescales.

The paper layout is as follows. In Sect. 2, we introduce the solid Earth model employed in this research, provide a detail account of model tuning procedure, and describe all of the required model input data. In Sect. 3, we present modeling results of the future bedrock topography, and assess the relative importance of the past and future ice load changes. In Sect. 4, we quantify the influence of predicted change in Antarctic bed topography on several aspects of ice sheet dynamics. Finally, in Sect. 5, we summarize key conclusions of broader interests.

2 Model and data

Ivins et al. (2013) presented a much improved ice loading history for the AIS since the LGM. As for the future, the recently concluded SeaRISE (Sea-level Response to Ice Sheet Evolution) project (Bindschadler et al., 2013; Nowicki et al., 2013) provided quantitative projections of the evolution of AIS under ongoing climate warming. We employ the new GIA capability (Ivins and James, 1999) of ISSM (Larour et al., 2012b), hereinafter referred to as the ISSM/GIA model, to combine these data of past and future ice loadings and calculate the first-order estimates of the change in bedrock topography over the same timescale projections as in the SeaRISE studies. Using appropriate analytical and numerical models, we then evaluate the stabilizing or destabilizing influence of predicted changes in bed topography on the ice sheet dynamics. While the SeaRISE experiments employed state-of-the-art numerical treatments of ice flow, it should be noted that none of these were coupled to the comprehensive solid Earth model, and hence were not in a position to perform such analysis.

2.1 The ISSM/GIA model

ISSM is a continental-scale, high-resolution, multi-model simulation code developed for understanding the dynamic behavior of large ice sheets (Larour et al., 2012b). This open source finite-element software is capable of simulating ice-flow mechanics of varying degrees of complexity (Seroussi et al., 2012), performing sensitivity analysis (e.g., Larour et al., 2012a), inverting unknown field parameters (e.g., Morlighem et al., 2010), and assessing mechanics of rift propagation and eventual collapse of ice shelves (e.g., Borstad et al., 2012). Semi-analytical GIA solution of Ivins and James (1999) is one of the several new features being actively implemented in ISSM. Here we briefly summarize the key elements of the model.

We assume that the ice sheet rests on top of the solid Earth, which is considered to be a simple two-layered incompressible continuum with upper elastic lithosphere floating on the viscoelastic (Maxwell material) mantle half-space. Theory governing the deformation of pre-stressed solid Earth subject to a normal surface traction of ice sheet relies upon the fundamental equations of motion and is discussed elsewhere (e.g., McConnell, 1965; Wolf, 1985; Ivins and James, 1999). For axisymmetric loading problems, it is possible to obtain the semi-analytical solution of vertical displacement at the ice/bedrock interface. This is the essence of the solution for GIA assessment. The GIA solutions perturb ice/bedrock contact surface within the area of ice sheet grounding. For the AIS that is surrounded on most of its periphery by floating ice, however, the extent of the grounded ice may evolve, as we assume in this study, according to the hydrostatic balance between the ice shelf and ocean water.

Given the appropriate ice loading history and choice of model/material parameters (cf. Sect. 2.2), the GIA solution depends on the size of ice load itself and the radial distance of evaluation point from the load centre. Assumed axisymmetry implies that the shape of ice load be essentially cylindrical (e.g., Ivins and James, 1999). In the Cartesian frame of ISSM/GIA model, we treat the size of ice load as the property of mesh element and compute the GIA solution at each node of the element. Individual 2-

D (xy-plane) mesh elements are defined as the equivalence of footprint (i.e., projection onto the xy-plane) of cylindrical disc loads, ensuring that the corresponding element and disc both share the same origin and plan-form area. The height of ice load is then assigned to each element such that the average normal tractional force on the corresponding area of ice/bedrock contact is conserved. At each node within the domain, the final GIA solutions are computed by integrating the solutions due to individual disc loads, defined as the property of mesh elements.

The ISSM/GIA model is tested against the benchmark experiments (Wolf, 1985; Ivins and James, 1999) and found to be sensitive to the mesh resolution. For reasonably fine resolution (element size typically on the same order of magnitude as ice thickness, or two orders of magnitude smaller than the characteristic size of ice sheet), however, the model performs well within the acceptable accuracy. Sample results are provided in Supplement Fig. S1.

2.2 Model tuning

We apply the ISSM/GIA model to the AIS. We mesh the footprint of present-day AIS (Bamber et al., 2009) into triangular elements. In order to capture the potentially interesting features, the domain is discretized to consist of high-resolution mesh around the coast (typical element size of 10 km) than inland Antarctica (element size of 25 km). This unstructured mesh captures the model inputs (e.g., past or future ice loads) in sufficient detail and provides a reasonable compromise between solution accuracy and computational efficiency. Doubling the mesh density, for example, improves the GIA solution (under present-day ice loading) only slightly (< 0.1 %), but it requires high computational cost by one order of magnitude.

We tune our model by testing it against 18 high-precision modern global positioning system (GPS) measurements (Thomas et al., 2011). In order to make reasonable predictions of the present-day GIA uplift, slow response of highly viscous solid earth demands that the evolution of AIS during the past several thousand years be considered in the ISSM/GIA model. There are a few reliable GIA ice loading histories for Antarctica

(e.g., Peltier, 2004; Ivins and James, 2005; Whitehouse et al., 2012). These generally describe the timing and magnitude of deglaciation since the LGM based on geological and ice core data. In this study, we employ a much improved loading history discussed in Ivins et al. (2013). By upgrading the loading history of Ivins and James (2005) with recently available geochronological constraint data, the later model was able to provide a more accurate GIA correction to GRACE (Gravity Recovery and Climate Experiment) data measured over the period 2003–2012 AD.

We define the distribution of Antarctic ice thickness, $h(x,y,t)$ at any time, t, in the past or future as follows:

$$h(x,y,t) = h(x,y,0) + \Delta h(x,y,t), \quad (1)$$

where $h(x,y,0)$ is the present-day distribution of ice thickness (Bamber et al., 2009), and $\Delta h(x,y,t)$ is the differential ice height (DIH) at the defined time t with reference to present-day, i.e. $t = 0$. (As a general convention, we use $t < 0$ to denote the past, i.e. before present, and $t > 0$ for future.) Based on Ivins et al. (2013), we have DIHs available for 11 time stamps in the past (at −1, −2.2, −3.2, −6.8, −7.6, −11.5, −15, −17, −19, −21 and −102 kyr; see Supplement Fig. S2). Note that $t = -21$ kyr roughly corresponds to the LGM of the AIS, while −15 kyr marks the onset of deglaciation of the WAIS (e.g., Clark et al., 2009). For $t = -1$ kyr, we consider zero DIH that could be constrained using the recently available surface mass balance data (e.g., Verfaillie et al., 2012; Favier et al., 2013). However, this process is not straightforward because the magnitude and spatial distribution of ice flux during the periods of inferred mass balance are vastly unknown. Furthermore, we consider $t = -102$ kyr to mark the initial configuration for AIS as being identical to the present-day configuration. This implicitly assumes that the DIHs before the LGM have minimal impact on the current and future response of the solid Earth. (We demonstrate in Sect. 3.2 that this is indeed a valid assumption.) Note also that the ice loading on the ISSM/GIA model is assumed to vary in a piece-wise linear fashion between the adjacent time stamps.

The model and material parameters considered in this study approximate the preliminary reference Earth model (Dziewonski and Anderson, 1981) and are taken from Ivins et al. (2013) unless otherwise specified. For several lithosphere thickness, Ivins et al. (2013) performed a parameter-space study in their two-layer mantle model. Noting that 65 and 115 km may represent respectively the average thickness of lithosphere for the WAIS and EAIS, Ivins et al. (2013) provided appropriate combinations of the upper and lower mantle viscosity. Because the past (see Supplement Fig. S2) and future DIHs (cf. Sect. 2.3 and Supplement Fig. S3) indicate that the majority of changes occurs in the WAIS, we consider 65 km thick lithosphere in our model. We cannot pick the corresponding mantle viscosity from Ivins et al. (2013), as our model does not have two mantle layers. We therefore consider the mantle viscosity as a tuning parameter, such that the difference in mean between the measured modern GPS data (Thomas et al., 2011) and modeled current GIA uplift at 18 data points is minimized (Fig. 2b). The optimized solutions for current uplift rate are shown in Fig. 2a. Key characteristic features of our predictions include greater uplift rate around the Ellsworth Mt. territory and a mild rate of bed subsidence in the interior of EAIS. Such spatial patterns of uplift rate essentially reflect signatures of the employed ice loading history (cf. Supplement Fig. S2). Note that the optimal predictions of uplift rate (Fig. 2a) correspond to a mantle viscosity of 7×10^{20} Pas. As expected, this magnitude falls in between the upper and lower mantle viscosity recommended for the chosen lithosphere thickness (Ivins et al., 2013). While the architecture of the ISSM/GIA model can capture high-resolution spatial variability in solid Earth material parameters, we do not experiment with lateral inhomogeneities in this study.

2.3 Future ice loading

The AIS mass change may become more dynamic in the future due to ice shelf melting (e.g., Pritchard et al., 2012; Depoorter et al., 2013; Rignot et al., 2013). The SeaRISE participating ice sheet models, primarily driven by melt-dominated forcing, quantified the future evolution of AIS under the proxy representative concentration pathway emis-

sion scenario 8.5 (RCP 8.5) (Bindschadler et al., 2013; Nowicki et al., 2013). The RCP 8.5 scenario represents an ongoing rise in emissions throughout the century, reaching 8.5 $W m^{-2}$ at 2100 AD (e.g., van Vuuren et al., 2011). The radiative forcings associated with RCP 8.5 scenario are loosely related to all three components of the SeaRISE model forcing, namely the surface climate, basal sliding and ice shelf melting. As these forcings are the ones that govern the future evolution of AIS, it is relevant in the present context to provide a brief account of them.

Firstly, the SeaRISE surface climate forcing follows 1.5 × A1B scenario (IPCC-AR4, 2007) until 2200 AD. (The A1B scenario generally describes a future world of rapid growth in economy, population that peaks in mid-century, and technologies that rely equally on both fossil and non-fossil sources of energy.) A mild increase in surface temperature, a total of 0.5 °C, is assumed during the period 2200–2500 AD. Secondly, no sliding amplification is considered until 2100 AD assuming that the Antarctic surface temperature will remain below zero, thus ignoring potential for surface melt induced basal sliding prior to this time. Thereafter, sliding increases linearly at the rate of 20 % of its original value per century, but only in coastal regions. Inland, the sliding amplification factor decreases linearly as a function of surface elevation such that no sliding enhancement is applied above 1200 m a.s.l. Thirdly, ice shelf melting is assumed to increase linearly from its present-day value to 60 m yr^{-1} at 2200 AD. Additional 10 m yr^{-1} melt extends linearly over the next 300 yr. Changes in basal melting conditions are only applied to the Amundsen Sea Sector (90–120° W) and Amery Ice Shelf (60–75° E), not to the Weddell and Ross Seas. Such a restriction of ice shelf melting considered in the SeaRISE experiment seems reasonable with reference to current observations (Depoorter et al., 2013; Rignot et al., 2013) that reveal that ice shelves around the Amundsen Sea are the most susceptible to melting. Furthermore, spatial distribution of ocean temperature anomalies (e.g., Pritchard et al., 2012) also supports this hypothesis.

Under the proxy RCP 8.5 scenario, a total of four ice sheet models simulates the future evolution of the AIS through 2500 AD. These models are the Anisotropic Ice Flow Model (AIF) (Wang et al., 2012), the Penn State Ice Sheet Model (PennState) (Pollard

and DeConto, 2009), the Potsdam Parallel Ice Sheet Model (PISM-PIK) (Winkelmann et al., 2011), and the Simulation Code for Polythermal Ice Sheets (SiCoPolIS) (Greve, 1997). These ice sheet models employ different assumptions and methods for solving the full physics involved in simulating ice flow (e.g., shallow-ice vs. first-order flow mechanics; different treatments for basal sliding, subglacial hydrology, and GL migration), they employ different numerics (e.g., different spatial and temporal resolutions), they have unique techniques for dealing with the prescribed model forcings, ad nauseam (cf. Bindschadler et al., 2013; Nowicki et al., 2013). Consequently, each ice sheet model produces a unique evolution of the AIS. We extract the DIHs from each model prediction for five time stamps (at 100, 200, 300, 400 and 500 yr); examples of future DIHs are provided in Supplement Fig. S3. The future ice loading for each model is then obtained from Eq. (1). Again, ice loads in the ISSM/GIA model are assumed to vary linearly between the adjacent time stamps.

3 Future bed topography

In order to predict the future bed topography for AIS, the calibrated ISSM/GIA model (cf. Sect. 2.2) is forced by an appropriate sequence of ice load changes into the future. As we have four independent sets of future ice loadings (cf. Sect. 2.3), we may compute four unique GIA solutions at any evaluation time in the future. Based on these solutions, here we present the first-order estimates of future bed uplifts, isolate the role of past and future ice loadings, and also evaluate how predicted change in bed topography alters the bedrock slope.

3.1 Vertical bed displacement

The GIA solutions for individual future ice loadings, combined with the consideration of a lone spin-up loading history, are computed at 2100 and 2500 AD and shown in Supplement Figs. S4 and S5, respectively. Although these solutions differ from each other

in both magnitude and their spatial distribution, some common features are noteworthy: (i) all models predict minor subsidence in a few places, particularly along the Wilkes Land; (ii) the topography of the interior of the EAIS is likely to remain unchanged, except for the PISM-PIK simulation at 2500 AD; and (iii) a pervasive and large uplift is predicted in the WAIS (except for the AIF simulations) and around the Amery Ice Shelf. We can, of course, offer no one GIA solution as being more reliable than any other. We therefore calculate the model average solutions (Fig. 3a and b) and consider these as the first-order estimates of the Antarctic bed uplift. It is possible that our ensemble approach for these predictions is insufficient. Nonetheless, we assert that they provide the correct order-of-magnitude estimates and the likely spatial patterns of the future bed uplift, which are sufficient to evaluate some of the IS/SE interactions outlined in Sect. 1.3.

By 2100 AD, the Amundsen Sea Sector and Amery Ice Shelf may rise by about four meters (Fig. 3a). Rest of the WAIS is likely to rise by up to two meters. The interior of the EAIS is predicted to remain unchanged. The Adelie and Wilkes Lands, where all ice sheet models predict the large snow accumulation (Nowicki et al., 2013), are likely to subside by about less than one meter. It should be noted that, for the chosen climate change scenario, all ice sheet models but SiCoPolIS predict moderate snow accumulation in the Queen Maud, Ross and Weddell basins, and minimal accumulation in the Amundsen and Amery basins (cf. Nowicki et al., 2013). Roughly similar spatial patterns of GIA uplift are predicted for 2500 AD as well (Fig. 3b). In this case, the bed may uplift by about 25 m in the Amundsen Sector, and by about 10–15 m in the rest of WAIS and Amery Ice Shelf. The interior of EAIS may also uplift by a few meters. Significant bed subsidence (about four meters) is likely to occur along the Adelie and Wilkes Lands, as well as along the coast north of Amery Ice Shelf.

We also find similar spatial patterns for the model average bed uplift rates (cf. Supplement Fig. S6). At 2100 AD, Amundsen Sea Sector and Wilkes Land are predicted to rise and subside at the highest rate of about 45 and $-5\,\mathrm{mm\,yr^{-1}}$, respectively. The interior of Marie Byrd Land is predicted to rise at the highest rate of $70\,\mathrm{mm\,yr^{-1}}$ at

2500 AD; Amundsen Sea Sector also rises at large rate of more than $50\,\mathrm{mm\,yr^{-1}}$. The greatest rate of subsidence (of about $-10\,\mathrm{mm\,yr^{-1}}$) is predicted along the east coast except around the Amery Ice Shelf.

At both evaluation times, as noted earlier, we obtain different GIA solutions associated with individual future ice loadings. Here we briefly outline how well these predictions for the Antarctic bed uplift match one another. The standard deviation shown in Fig. 3c illustrates that the model predictions are generally in good accord with each other at 2100 AD, except around the Amundsen Sector and Amery Ice Shelf. As depicted in Fig. 3d, however, relatively poor agreement is found amongst the model predictions at 2500 AD. Large deviations are predicted once again around the Amundsen Sea Sector. Moderate deviations can be seen in the Ross and Ronne Ice Shelves, as well as along the east coast including the Amery Ice Shelf. Such deviations amongst model predictions for the Antarctic bed topography predicted both at 2100 and 2500 AD can generally be attributed to the limiting values of GIA solutions predicted by the PennState and AIF models (cf. Supplement Figs. S4 and S5).

It needs to be mentioned here that we do not model the subglacial erosion in this study, although quite rapid evacuation of soft sediments is now occurring at the bed of Pine Island Glacier. Erosion has been roughly estimated to cause the topography to lower at a rate of $0.6 \pm 3\,\mathrm{m\,yr^{-1}}$ as ice flow exceeding $1\,\mathrm{km\,yr^{-1}}$ erodes material in deep longitudinal fjord valleys (Smith et al., 2012). This erosive action typically takes place in 20 km wide valleys of approximately 200 km length. While an important consideration in ice sheet modeling (Kessler et al., 2008), GIA topographic responses occur over much broader length scales exceeding the areal dimensions of fast erosion by nearly two orders of magnitude, thus having an impact on the evolution of the ice sheet at the scale of the drainage basin itself.

3.2 Role of past and future loadings

Our predictions of bed uplift reflect the combined effects of long-term viscous creep of solid Earth driven by the ice loading history and its short-term (centennial timescales) viscoelastic response to the future ice load change. It might be useful to isolate the contribution of past and future ice loadings on the evolution of future bed topography. First, we let the calibrated ISSM/GIA model (driven by the past loading alone) run for the next 500 yr into the future under the idealized condition that the current distribution of ice thickness prevails as is, thus imposing $\Delta h(x,y,t) = 0$ m for all $t \in [0,500]$ yr. We find similar spatial patterns of bed uplift, as shown in Fig. 2a for the current uplift rate, in the future; the total amount of GIA uplift by the next 100 and 500 yr are in the respective ranges of about $[-0.1, 0.5]$ (Fig. 4a) and $[-0.5, 2.5]$ m (Fig. 4b). In such an idealized scenario of the unchanged future AIS, the notable observations are that the Peninsula, whole of WAIS, and coastal regions of EAIS are likely to uplift, with the highest uplift occurring around the Ellsworth Mt. territory, and that the interior of the EAIS may remain unaffected or subside minimally. These are consistent with characteristic features of the employed ice loading history (cf. Supplement Fig. S2).

Next, we compute model average GIA solutions at years 2100 AD (Fig. 4c) and 2500 AD (Fig. 4d) by perturbing the steady-state response of solid Earth to present-day AIS loading through imposition of the future ice load changes. Alternative solutions are found by subtracting the GIA solutions associated with the past loading alone (Fig. 4a and b) from the corresponding final predictions (Fig. 3a and b). Thus obtained solutions are essentially identical with those shown in Fig. 4c and d, implying that the principle of superposition holds (cf. Supplement Fig. S7).

Comparing the estimates of GIA uplift associated with the past (Fig. 4a and b) and future ice loadings alone (Fig. 4c and d) with those depicted in Fig. 3a and b, we find that the future ice loading dominates and that the contribution of long-term viscous creep is only about one tenth the magnitude of the predicted GIA uplifts. This suggests that the errors associated with the ice loading history may have minor consequences on

the future predictions of the Antarctic bed topography, provided the differing scenarios properly sample the possible amplitude of the ice sheet loading. Significant changes in magnitude and timing of the loading history may, however, require that the different mantle viscosity be employed in the ISSM/GIA model to correctly predict the current uplift rates (cf. Sect. 2.2). This, in turn, may yield the different contribution (not necessarily higher) of long-term viscous creep of the solid Earth to predictions of the future bed uplift. Nonetheless, it is important here to highlight the need for better constraining the DIHs, particularly in the recent past (during the past 1 kyr).

3.3 Change in bed slope

Strong spatial variability in the future GIA uplift (cf. Sect. 3.1) implies that the Antarctic bed slope will be modulated in the future (e.g., Gomez et al., 2013). We compute current and future bedrock slopes (associated with the model average GIA solutions) following $\alpha_b(x,y,t) = \sqrt{\alpha_{bx}^2(x,y,t) + \alpha_{by}^2(x,y,t)}$, where $\alpha_{bx}(x,y,t)$ and $\alpha_{by}(x,y,t)$ are the x and y components of the bed slope, respectively. Figure 5b, for example, depicts the present-day bedrock slope of Antarctica. While this plot reveals the degree of bed steepness, it does not provide the information regarding the aspect of slope. It is important to identify whether the bedrock has forward or reverse slope, particularly while evaluating the role of GIA uplift on the marine ice sheet instability (to be discussed later). We therefore plot the current bathymetry of the AIS in Fig. 5a; in order to facilitate the discussion, we only consider the areas with bedrock below sea level. Notice in the figure, for example, the blue color around the interior of WAIS that illustrates the existence of reverse bed in those regions.

We obtain the future bedrock topography by adding the current bedrock topography and the future GIA solution (Sect. 3.1). From the corresponding bedrock topography, we calculate the bed slope at 2100 and 2500 AD. The changes in bedrock slope are then computed by subtracting the present-day slope (Fig. 5b) from the future bed slope. Sample results are shown in Fig. 5c for 2500 AD. In the figure, we generally notice the

reduced bed slope (apart from a few localized regions with enhanced slope) around the Amundsen Sea Sector and Amery Ice Shelf where large uplifts are predicted. The reverse bed in these regions will thus have generally less steep slope in the future. Similar spatial patterns (but small magnitudes) of change in bed slope are obtained for 2100 AD as well (results not shown).

Although the magnitudes of change are larger in the regions where the bed has experienced large uplift, such as in the Amundsen Sea Sector and Amery Ice Shelf, per cent changes in bed slope are significant also around the Ronne and Ross Ice Shelves (Fig. 5d). The bedrock slopes beneath these ice shelves, for example, reduce by more than one percent at 2500 AD. Such changes in the Antarctic bed slope beneath and around the large ice shelves may impact the magnitude of GL migration (cf. Sect. 1.1 and Fig. 1a) and thus future dynamics.

4 Implications for ice sheet dynamics

Our predictions for the future evolution of Antarctic bed topography may influence the future dynamics of AIS. In this section, we specifically quantify how the predicted change in bed topography affects the gravitational driving stress (Sect. 4.1), GL migration (Sect. 4.2), and ice surface velocities (Sect. 4.3). Because our model is not yet capable of computing IS/SE interactions with full dynamic feedbacks, it should be noted that some of the results presented below are obtained by bootstrapping the relevant future bedrock topography. The general procedure includes the following. First, we consider the present-day settings (geometric setting and boundary conditions) of the AIS for our calculations. Next, we upgrade the geometry and relevant boundary conditions to account for the future GIA uplifts and perform recalculations. Comparing corresponding results, we finally isolate the influence of GIA uplifts. We advise caution in overinterpreting any individual results, obtained from the present-day settings of AIS perturbed by the future GIA uplifts, for 2100 and 2500 AD.

4.1 Gravitational driving stress

Here, we discuss the GIA effects on the gravitational driving stress. We compute driving stress following $\tau_{\mathrm{d}}(x,y,t) = \sqrt{\tau^2_{\mathrm{d}x}(x,y,t) + \tau^2_{\mathrm{d}y}(x,y,t)}$, where $\tau_{\mathrm{d}x}(x,y,t)$ and $\tau_{\mathrm{d}y}(x,y,t)$ are the x and y components of the driving stress, respectively. For $i = x,y$, we define $\tau_{\mathrm{d}i}(x,y,t) = \rho\, g\, h(x,y,t)\, \alpha_{\mathrm{s}i}(x,y,t)$ as the ith component of driving stress (e.g., Cuffey and Paterson, 2010), where ρ (= 917 kg m^{-3}) is the ice density, g (= 9.81 m s^{-2}) is the gravitational acceleration, and $\alpha_{\mathrm{s}i}$ is the ith component of surface slope. As noted earlier, we use the present-day ice thickness, i.e. $h(x,y,t) = h(x,y,0)$, in all calculations. Hence, the change in surface slope due to the GIA uplift is responsible for modulating the driving stress.

Figure 6 shows the change in driving stress associated with the bed uplifts predicted at years 2100 and 2500 AD. In both cases (Fig. 6a and b), we notice small but similar trends of change in driving stress. Although the maximum changes in driving stress are about three orders of magnitude smaller than the driving stress itself, large changes are predicted at positions of larger bed uplift. Reduction in driving stress is evident around the Amery Ice Shelf, implying that the local surface slopes are likely to flatten in this region. Minor increments in driving stress are predicted in the area around Dome C. Complex patterns are predicted around the Amundsen Sea Sector; an extensive zone of reduced driving stress is surrounded by zones with enhanced driving stress (see particularly Fig. 6b).

Theoretically, for the given distribution of ice thickness, changes in bed slope and surface slope (and, hence, the driving stress) should be in phase for the topography with forward slope, but in out of phase for cases with reverse slope. Due to the complex nature of the Antarctic bathymetry, it is an arduously difficult task to find a robust and consistent relationship between changes in bed slope and driving stress, particularly around the Amundsen Sector (compare, for example, Figs. 5c vs. 6b). Nonetheless, we generally find the reduction in local driving stress associated with the GIA uplift (compare, for example, Figs. 3b vs. 6b). Given the small order-of-magnitude predictions

for change in driving stress (i.e., several hundreds of Pascal only), it is important here to note that, as will also be shown in Sect. 4.3, minor changes in driving stress may affect substantially the ice sheet dynamics as ice velocities are directly propertional to the driving stress by about a power of three (e.g., Cuffey and Paterson, 2010).

4.2 GL migration

In this section, we evaluate the effects of GIA uplift on the GL. We employ the simple hydrostatic equilibrium criterion to identify the transition points by seeking the floating ice thickness, $h_f(x,y,t)$, such that

$$\rho\ h_f(x,y,t) = -\rho_w\ b(x,y,t), \tag{2}$$

where ρ_w (= 1028 kg m^{-3}) is the ocean water density, and $b(x,y,t) < 0$ is the bedrock elevation (with respect to mean sea level) of the marine portions of the ice sheet. Regions with ice thickness $h(x,y,t) > h_f(x,y,t)$ are assumed to be grounded and the rest to be floating. Because we use the present-day ice thickness, i.e. $h(x,y,t) = h(x,y,0)$, in all calculations, the extent of the current and future grounded ice (i.e., GL) is determined by the corresponding bathymetry.

Using Eq. (2), we compute the extent of the grounded ice for t = 0, 100, and 500 yr. Changes in GL are then identified by subtracting, in turn, the first solution from the latter two. Figure 7a, for example, shows the GL migration associated with the GIA uplift predicted for 2500 AD. The mask shown in the figure primarily represents GL advance, implying that more ice will be grounded in the future due to the GIA effects. However, we also predict the minor GL retreat in a few scattered locations, particularly around the Wilkes and Queen Mary Lands, where the bedrock is generally predicted to subside partly due to the large snow accumulation simulated under the chosen climate change scenario (Nowicki et al., 2013). Note that we also obtain similar but less extensive migration in GL associated with the GIA uplift predicted for 2100 AD (results not shown); there is however no evidence of GL retreat in this case.

Based on the measured ice surface velocities (Rignot et al., 2011), we locate about 2800 ice flowlines to quantify the magnitude of GL migration (mostly advance) associated with the predictions of GIA uplift at 2500 AD. Results are shown for three important regions, namely the Amery (Fig. 7b), Ross (Fig. 7c) and Ronne (Fig. 7d) Ice Shelves. Figures reveal that the GL may advance by more than 50 km in the Amery Ice Shelf and 100 km in other two ice shelves. Significant GL advance (by tens of km) is also predicted in the Amundsen Sector, Larsen Ice Shelf, Brunt Ice Shelf, and in other regions. In a few locations, e.g. Shackleton Ice Shelf in the Queen Mary Land, as noted earlier we notice the minor retreat (by $\approx$ 10 km) of the GL.

Although the primary control of GL migration in our calculations is bedrock elevation (Eq. 2), it should be noted that the bedrock slope plays an equally important role (e.g., Lingle and Clark, 1985; Gomez et al., 2010) as summarized in Sect. 1.1. Extensive observation of the GL advance associated with the GIA uplift is generally consistent with what is expected when bed slope reduces in the reverse topography (compare Fig. 5a vs. c, for example, around the Ronne Ice Shelf). For bedrock with forward slopes, however, the advancement in GL can be explained by the GIA induced increment in bed slopes (compare Fig. 5a vs. c, for example, around the Getz Ice Shelf). The minor GL retreat predicted, for example, in Shackleton Ice Shelf is associated with the flattening (Fig. 5c) of the forward bed slope (Fig. 5a). Although we are able to show a systematic relationship amongst the bathymetry, change in bed slope, and the direction of the GL migration in a few cases, it is complicated to provide such one-to-one relationships consistently over the entire ice sheet. Nonetheless, the results lend the confidence to conclude that the GIA effects generally support the extension of grounded ice (i.e., GL advance) in the future, thereby promoting the stability to the marine portions of the ice sheet that rest on a reverse bed slope.

4.3 Ice surface velocities

Finally, we analyze the influence of GIA uplift on the ice surface velocities. By solving the quasi-static thermomechanical problem of ice flow, we calculate the englacial

velocity field of the AIS with and without GIA effects. We assume that higher-order physics based on the equations governing mass and momentum conservation (Pattyn, 2003) together with the constitutive relations for isotropic ice (Glen, 1955) describe the internal creep deformation of ice, and that a viscous law of friction (e.g., MacAyeal, 1993) governs basal sliding. We rely on a steady-state thermal problem identical for all simulations, based on present-day conditions. For simplicity, we do not consider the possibility of till deformation underneath the ice sheet. Description of ice rheology (Glen, 1955) and other common assumptions related to ice flow modeling can be found elsewhere (e.g., Cuffey and Paterson, 2010).

For the present-day setting of the AIS, we solve this problem of ice dynamics through diagnostic simulation of the 3-D ice flow capability of ISSM, satisfying a number of boundary conditions (e.g., Larour et al., 2012b). We impose: (i) stress-free condition at the ice/atmosphere interface; (ii) water pressure directing towards the ice sheet at the ice/ocean (peripheral) interface; and (iii) sliding condition governed by the basal friction at the ice/bed interface. Zero friction is applied at the base of ice shelf (i.e., free-floating condition), while basal friction under the grounded ice is inferred from InSAR (Interferometric Synthetic Aperture Radar) based surface velocities (Rignot et al., 2011) using a data assimilation technique (e.g., Morlighem et al., 2010). The basal friction pattern is similar to the one described in Morlighem et al. (2013).

We re-run the simulation for two additional cases, associated with the predictions of GIA uplift at years 2100 and 2500 AD. In each case, we upgrade the bedrock and surface elevations of the grounded ice; the extents of the grounded ice (GLs) are also updated (cf. Sect. 4.2). For floating ice as well, we upgrade both bed and surface elevations so that all floating ice is in hydrostatic equilibrium, which ensures continuity of the driving stress at GL. Applying the same boundary conditions discussed above (except in the newly grounded areas), we compute the englacial velocity for both cases associated with the future GIA uplifts. In areas previously floating that become grounded at t = 100 and 500 yr (cf. Fig. 7a), we assume that basal stress is equal to the gravitational driving stress as a first-order approximation to update basal friction (Morlighem et al., 2013).

For a given vertical profile of ice sheet, the maximum velocity is always observed at the surface. We therefore place our emphasis upon the GIA effects on the ice surface velocities. Using the simulation results discussed above, we compute the GIA induced change in surface velocity associated with the predictions of GIA uplifts at years 2100 AD (Fig. 8a) and 2500 AD (Fig. 8b). In both cases, we find similar patterns of change in ice surface velocity. Although the predicted changes are small, about two to three order-of-magnitude smaller than the surface velocities themselves (Rignot et al., 2011), a systematic reduction in velocity is evident around the sheet/shelf margins. This suggests that the GIA effects generally contribute to decelerating the flow speed across the GL, and hence promotes stability to the marine portions of the ice sheet. Note that we mask out the ice shelves in our figures for we have no intention of making predictions in the ice shelves.

The predicted changes in surface velocity for the grounded ice can be interpreted as the combined effects of changes in driving stress (cf. Sect. 4.1 and Fig. 6) and the GL (cf. Sect. 4.2 and Fig. 7) associated with the GIA uplifts. Around the Ross and Ronne Ice Shelves, the GIA induced reduction in surface velocity is consistent with the GL advance. In other regions, e.g. Amundsen Sea Sector and Amery Ice Shelf, predicted reduction in ice velocity can be attributed partly to the GL advance and partly to the reduced driving stress. All in all, effects of GIA on several aspects of ice dynamics (e.g., driving stress, GL, and ice surface velocities) are consistent in that the GIA promotes a systematic stability to marine portions of the AIS in the future.

5 Conclusions

This study has examined the interplay between the ice sheet evolution and the solid Earth responses for the AIS. First, we compute the future uplift of the Antarctic bedrock using the calibrated ISSM/GIA model driven by the inferred and predicted evolution of

the ice sheet. Next, we evaluate how such a response of the solid Earth impacts on the dynamics of the AIS.

Our calculations are based on several approximations of model physics and numerics; it is important to highlight some of these here. The employed GIA model describes a simple two-layer representation of the solid Earth; the model and material parameters are kept constant spatially. Our ice sheet model solves the quasi-static thermomechanical flow problem for higher-order mechanics; the GLs are determined by hydrostatic equilibrium criterion. A more comprehensive exploration of the positive or negative IS/SE feedbacks will be warranted in the future. There is much to be learned for additional constraints on the GIA models that employ additional GPS data, possibly right in the heart of the Amundsen Sea Sector where viscoelastic uplift rates may approach 40 mm yr^{-1} (Groh et al., 2012). Our computations of ice loading after the present-day rely on several ice sheet models driven by the melt-dominated forcing under the proxy RCP 8.5 emission scenario. The model average GIA response thus computed provides our assessment of its impact on the ice sheet dynamics. Given these limitations associated with the data and methods, this research nonetheless reaches the following two important conclusions of broader interest.

First, the short-term viscoelastic response of the solid Earth to the future ice load change, rather than its long-term viscous response to the past loading, governs the future evolution of the Antarctic bed topography. The magnitude and spatial variability in the future bed uplift are therefore determined by the nature of future evolution of the AIS. A larger uplift is expected, for example, where the ice sheet loses more mass, while its far-field consequences seem to involve a relatively small amplitude subsidence. Our calculations suggest that the Antarctic bed may rise by a few meters and a few tens of meters around the WAIS, particularly the Amundsen Sea Sector, and Amery Ice Shelf at years 2100 and 2500 AD, respectively. Minor subsidences of about one meter and a few meters are predicted along the Wilkes Land at the respective times, partly caused by the net accumulation in the climate scenario runs (Nowicki et al., 2013). The interior of the EAIS is likely to remain unchanged.

Second, a pervesive and large uplift predicted in the interior of the WAIS, a substantially marine-based ice sheet, has particular significance because it corresponds to the flattening of the reverse bed slope. This drives the GL forward and consequently promotes the stability to the ice sheet. Our calculations, based on the present-day setting of the AIS perturbed by the future GIA uplift, reveal that the GL may advance by greater than 100 km in the Ross and Ronne Ice Shelves due to the predicted GIA uplift for 2500 AD. This may reduce the future ice surface velocities across the GLs by several tens of meter per annum.

The conclusions summarized above indicate a negative feedback between the ice sheet evolution and the solid Earth response for the marine ice sheet. For reverse beds, for example, loss in ice mass flattens the bed and drives the GL forward and hence decelerates the rate of mass loss. Although our model is capable of illustrating this mechanism systematically, accurate quantification of its significance requires a dynamically coupled IS/SE model. This negative feedback is consistent with the ice sheet and sea level simulations computed by Gomez et al. (2010, 2013) wherein loss in ice mass reduces the local sea level due to self-gravitation and hence decelerates the rate of mass loss. For accurate simulations of the AIS on centennial timescales under the reasonable climate change scenarios, both the solid Earth and sea level changes proximal to the GL may need to be properly accounted for.

Supplementary material related to this article is available online at http://www.solid-earth-discuss.net/6/191/2014/sed-6-191-2014-supplement.pdf.

Acknowledgements. This study was performed at the Caltech's Jet Propulsion Laboratory under a contract with the NASA's Cryosphere Science and the Solid Earth Surface and Interior Focus Area Programs. Authors are indebted to the SeaRISE participants for providing them with the valuable data. S. Adhikari is thankful to V. Tsai for hosting him as a postdoctoral scholar at Caltech, which made the completion of this writeup possible.

References

Bamber, J. L. and Aspinall, W. P.: An expert judgement assessment of future sea level rise from the ice sheets, Nat. Clim. Change, 3, 424–427, 2013. 192

Bamber, J. L., Gomez-Dans, J. L., and Griggs, J. A.: A new 1 km digital elevation model of the Antarctic derived from combined satellite radar and laser data – Part 1: Data and methods, The Cryosphere, 3, 101–111, doi:10.5194/tc-3-101-2009, 2009. 198, 199

Bindschadler, R., Nowicki, S., Abe-Ouchi, A., Aschwanden, A., Choi, H., Fastook, J., Granzow, G., Greve, R., Gutowski, G., Herzfeld, U., Jackson, C., Johnson, J., Khroulev, C., Levermann, A., Lipscomb, W., Martin, M., Morlighem, M., Parizek, B., Pollard, D., Price, S., Ren, D., Saito, F., Sato, T., Seddik, H., Seroussi, H., Takahashi, F., Walker, R., and Wang, W.: Ice-sheet model sensitivities to environmental forcing and their use in projecting future sea-level (the SeaRISE project), J. Glaciol., 59, 195–224, doi:10.3189/2013JoG12J125, 2013. 193, 196, 201, 202, 223, 228

Borstad, C. P., Khazendar, A., Larour, E., Morlighem, M., Rignot, E., Schodlok, M. P., and Seroussi, H.: A damage mechanics assessment of the Larsen B ice shelf prior to collapse: toward a physically-based calving law, Geophys. Res. Lett., 39, 1–5, doi:10.1029/2012GL053317, 2012. 197

Clark, P. U., Dyke, A. S., Shakun, J. D., Carlson, A. E., Clark, J., Wohlfarth, B., Mitrovica, J. X., Hostetler, S. W., and Marshall McCabe, A.: The last glacial maximum, Science, 5941, 710–714, doi:10.1126/science.1172873, 2009. 199

Conway, H., Hall, B. L., Denton, G. H., Gades, A. M., and Waddington, E. D.: Past and future grounding-line retreat of the West Antarctic Ice Sheet, Science, 286, 280–283, doi:10.1126/science.286.5438.280, 1999. 194

Cook, C., van de Flierdt, T., Williams, T., et al.: Dynamic behaviour of the East Antarctic ice sheet during Pliocene warmth, Nat. Geosci., 6, 765–769, doi:10.1038/ngeo1889, 2013. 193

Cuffey, K. and Paterson, W. S. B.: The Physics of Glaciers, 4th edn., Elsevier, 2010. 195, 208, 209, 211

Depoorter, M. A., Bamber, J. L., Griggs, J. A., Lenaerts, J. T. M., Ligtenberg, S. R. M., van den Broeke, M. R., and Moholdt, G.: Calving fluxes and basal melt rates of Antarctic ice shelves, Nature, 502, 89–92, doi:10.1038/nature12567, 2013. 200, 201

Dziewonski, A. M. and Anderson, D. L.: Preliminary reference Earth model, Phys. Earth Planet. In., 25, 297–356, 1981. 200

Favier, L., Gagliardini, O., Durand, G., and Zwinger, T.: A three-dimensional full Stokes model of the grounding line dynamics: effect of a pinning point beneath the ice shelf, The Cryosphere, 6, 101–112, doi:10.5194/tc-6-101-2012, 2012. 194

Favier, V., Agosta, C., Parouty, S., Durand, G., Delaygue, G., Gallée, H., Drouet, A.-S., Trouvilliez, A., and Krinner, G.: An updated and quality controlled surface mass balance dataset for Antarctica, The Cryosphere, 7, 583–597, doi:10.5194/tc-7-583-2013, 2013. 199

Fjeldskaar, W.: The amplitude and decay of the glacial forebulge in Fennoscandia, Norsk Geol. Tidsskr., 74, 2–8, 1994. 195

Glen, J.: The creep of polycrystalline ice, Proc. R. Soc. A, 228, 519–538, 1955. 211

Gomez, N., Mitrovica, J. X., Huybers, P., and Clark, P. U.: Sea level as a stabilizing factor for marine-ice-sheet grounding lines, Nat. Geosci., 3, 850–853, doi:10.1038/ngeo1012, 2010. 193, 194, 210, 214

Gomez, N., Pollard, D., and Mitrovica, J.: A 3-D coupled ice sheet–sea level model applied to Antarctica through the last 40 kyr, Earth Planet. Sc. Lett., 384, 88–99, 2013. 193, 195, 206, 214

Greve, R.: A continuum-mechanical formulation for shallow polythermal ice sheets, Philos. T. R. Soc. A, 355, 921–974, 1997. 202

Groh, A., Ewert, H., Scheinert, M., Fritsche, M., Rülke, A., Richter, A., Rosenau, R., and Dietrich, R.: An investigation of glacial isostatic adjustment over the Amundsen Sea Sector, West Antarctica, Global Planet. Change, 98–99, 45–53, 2012. 213

Hughes, T., Sargent, A., and Fastook, J.: Ice-bed coupling beneath and beyond ice streams: Byrd Glacier, Antarctica, J. Geophys. Res., 116, 1–17, doi:10.1029/2010JF001896, 2011. 195

IPCC-AR4: Fourth Assessment Report: Climate Change 2007: The AR4 Synthesis Report, Geneva: IPCC, available at: http://www.ipcc.ch/ipccreports/ar4-wg1.htm, 2007. 201

Ivins, E. R. and James, T. S.: Simple models for late Holocene and present-day Patagonian glacier fluctuations and predictions of a geodetically detectable isostatic response, Geophys. J. Int., 138, 601–624, doi:10.1046/j.1365-246x.1999.00899.x, 1999. 193, 196, 197, 198

Ivins, E. R. and James, T. S.: Antarctic glacial isostatic adjustment: a new assessment, Antarct. Sci., 17, 541–553, 2005. 199

Ivins, E. R., James, T. S., Wahr, J. O., Schrama, E. J., Landerer, F. W., and Simon, K. M.: Antarctic contribution to sea level rise observed by GRACE with improved GIA correction, J. Geophys. Res., 118, 3126–3141, doi:10.1002/jgrb.50208, 2013. 196, 199, 200, 222

Katz, R. and Worster, M.: Stability of ice-sheet grounding lines, Proc. R. Soc. A, 466, 1597–1620, doi:10.1098/rspa.2009.0434, 2010. 194

Kessler, M. A., Anderson, R. S., and Briner, J. P.: Fjord insertion into continental margins driven by topographic steering of ice, Nat. Geosci., 1, 365–369, doi:10.1038/ngeo201, 2008. 204

Larour, E., Schiermeier, J., Rignot, E., Seroussi, H., Morlighem, M., and Paden, J.: Sensitivity analysis of Pine Island Glacier ice flow using ISSM and DAKOTA, J. Geophys. Res., 117, 1–16, doi:10.1029/2011JF002146, 2012a. 197

Larour, E., Seroussi, H., Morlighem, M., and Rignot, E.: Continental scale, high order, high spatial resolution, ice sheet modeling using the Ice Sheet System Model (ISSM), J. Geophys. Res., 117, 1–20, doi:10.1029/2011JF002140, 2012b. 193, 196, 197, 211

Le Meur, E. and Huybrechts, P.: A comparison of different ways of dealing with isostasy: examples from modelling the Antarctic ice sheet during the last glacial cycle, Ann. Glaciol., 23, 309–317, 1996. 195

Le Meur, E. and Huybrechts, P.: A model computation of the temporal changes of surface gravity and geoidal signal induced by the evolving Greenland ice sheet, Geophys. J. Int., 145, 835–849, 2001. 195

Lingle, C. and Clark, J.: A numerical model of interactions between a marine ice sheet and the solid earth: application to a west Antarctic ice stream, J. Geophys. Res., 90, 1100–1114, 1985. 193, 194, 210

MacAyeal, D.: A tutorial on the use of control methods in ice-sheet modeling, J. Glaciol., 39, 91–98, 1993. 211

McConnell, R. K. J.: Isostatic adjustment in a layered Earth, J. Geophys. Res., 70, 5171–5188, doi:10.1029/JZ070i020p05171, 1965. 197

Morlighem, M., Rignot, E., Seroussi, H., Larour, E., Ben Dhia, H., and Aubry, D.: Spatial patterns of basal drag inferred using control methods from a full-Stokes and simpler models for Pine Island Glacier, West Antarctica, Geophys. Res. Lett., 37, 1–6, doi:10.1029/2010GL043853, 2010. 197, 211

Morlighem, M., Seroussi, H., Larour, E., and Rignot, E.: Inversion of basal friction in Antarctica using exact and incomplete adjoints of a higher-order model, J. Geophys. Res., 118, 1746–1753, doi:10.1002/jgrf.20125, 2013. 211, 212

Naish, T., Powell, R., Levy, G., et al.: Obliquity-paced pliocene West Antarctic ice sheet oscillations, Nature, 458, 322–329, doi:10.1038/nature07867, 2009. 193

Nowicki, S., Bindschadler, R., Abe-Ouchi, A., Aschwanden, A., Bueler, E., Choi, H., Fastook, J., Granzow, G., Greve, R., Gutowski, G., Herzfeld, U., Jackson, C., Johnson, J., Khroulev, C., Larour, E., Levermann, A., Lipscomb, W., Martin, M., Morlighem, M., Parizek, B., Pollard, D., Price, S., Ren, D., Rignot, E., Saito, F., Sato, T., Seddik, H., Seroussi, H., Takahashi, K., Walker, R., and Wang, W.: Insights into spatial sensitivities of ice mass response to environmental change from the SeaRISE ice sheet modeling project I: Antarctica, J. Geophys. Res., 118, 1–23, doi:10.1002/jgrf.20081, 2013. 196, 201, 202, 203, 209, 213, 223

Pattyn, F.: A new three-dimensional higher-order thermomechanical ice sheet model: basic sensitivity, ice stream development, and ice flow across subglacial lakes, J. Geophys. Res., 108, 1–15, doi:10.1029/2002JB002329, 2003. 193, 211

Peltier, W.: Global glacial isostasy and the surface of the ice-age Earth: The 699 ICE-5G (VM2) model and GRACE, Annu. Rev. Earth Pl. Sc., 32, 111–149, 2004. 199

Pollard, D. and DeConto, R.: Modelling West Antarctica ice sheet growth and collapse through the past five million years, Nature, 458, 329–332, 2009. 195, 201

Pritchard, H. D., Ligtenberg, S. R. M., Fricker, H. A., Vaughan, D. G., van den Broeke, M. R., and Padman, L.: Antarctic ice-sheet loss driven by basal melting of ice shelves, Nature, 484, 502–505, doi:10.1038/nature10968, 2012. 200, 201

Raymo, M., Mitrovica, J. X., O'Leary, M., DeConto, R., and Hearty, P.: Departures from eustasy in Pliocene sea-level records, Nat. Geosci., 4, 328–332, doi:10.1038/ngeo1118, 2011. 193

Rignot, E., Mouginot, J., and Scheuchl, B.: Ice flow of the Antarctic Ice Sheet, Science, 333, 1427–1430, doi:10.1126/science.1208336, 2011. 210, 211, 212

Rignot, E., Jacobs, S., Mouginot, J., and Scheuchl, B.: Ice shelf melting around Antarctica, Science, 341, 266–270, doi:10.1126/science.1235798, 2013. 200, 201

Schoof, C.: Ice sheet grounding line dynamics: steady states, stability, and hysteresis, J. Geophys. Res., 112, 1–19, doi:10.1029/2006JF000664, 2007. 194

Seroussi, H., Ben Dhia, H., Morlighem, M., Rignot, E., Larour, E., and Aubry, D.: Coupling ice flow models of varying order of complexity with the Tiling Method, J. Glaciol., 58, 776–786, doi:10.3189/2012JoG11J195, 2012. 197

Siegert, M., Ross, N., Corr, H., Kingslake, J., and Hindmarsh, R.: Late Holocene ice-flow reconfiguration in the Weddell Sea sector of West Antarctica, Quaternary Sci. Rev., 78, 98–107, 2013. 193, 194

Smith, A. M., Bentley, C. R., Bingham, R. G., and Jordan, T. A.: Rapid subglacial erosion beneath Pine Island Glacier, West Antarctica, Geophys. Res. Lett., 39, L12501, doi:10.1029/2012GL051651, 2012. 204

Thomas, I., King, M., Bentley, M. J., Whitehouse, P. L., Penna, N. T., Williams, S. D. P., Riva, R. E. M., Lavallee, D. A., Clarke, P. J., King, E. C., Hindmarsh, R. C. A., and Koivula, H.: Widespread low rates of Antarctic glacial isostatic adjustment revealed by GPS observations, Geophys. Res. Lett., 38, L22302, doi:10.1029/2011GL049277, 2011. 198, 200, 222

Thomas, R.: Thickening of the Ross Ice Shelf and equilibrium stat of the West Antarctic Ice Sheet, Nature, 259, 180–183, 1976. 193

van Vuuren, D., Edmonds, J., Kainuma, M., Riahi, K., Thomson, A., Hibbard, K., Hurtt, G., Kram, T., Krey, V., Lamarque, J., Masui, T., Meinshausen, M., Nakicenovic, N., Smith, S., and Rose, S.: The representative concentration pathways: an overview, Clim. Dynam., 109, 5–31, 2011. 201

Vaughan, D. and Arthern, R.: Why is it hard to predict the future of ice sheets?, Science, 315, 1503–1504, 2007. 193, 194

Verfaillie, D., Fily, M., Le Meur, E., Magand, O., Jourdain, B., Arnaud, L., and Favier, V.: Snow accumulation variability derived from radar and firn core data along a 600 km transect in Adelie Land, East Antarctic plateau, The Cryosphere, 6, 1345–1358, doi:10.5194/tc-6-1345-2012, 2012. 199

Walker, R. T., Holland, D. M., Parizek, B. R., Alley, R. B., Nowicki, S. M. J., and Jenkins, A.: Efficient flowline simulations of ice shelf-ocean interactions: sensitivity studies with a fully coupled model, J. Phys. Oceanogr., 43, 2200–2210, doi:10.1175/JPO-D-13-037.1, 2013. 193

Wang, W., Li, J., and Zwally, J.: Dynamic inland propagation of thinning due to ice loss at the margins of the Greenland ice sheet, J. Glaciol., 58, 734–740, 2012. 201

Weertman, J.: Stability of the junction of an ice sheet and an ice shelf, J. Glaciol., 13, 3–11, 1974. 194

Whitehouse, P., Bentley, M. J., and Brocq, A. M. L.: A deglacial model for Antarctica: geological constraints and glaciological modelling as a basis for a new model of Antarctic glacial isostatic adjustment, Quaternary Sci. Rev., 32, 1–24, 2012. 199

Winkelmann, R., Martin, M. A., Haseloff, M., Albrecht, T., Bueler, E., Khroulev, C., and Levermann, A.: The Potsdam Parallel Ice Sheet Model (PISM-PIK) – Part 1: Model description, The Cryosphere, 5, 715–726, doi:10.5194/tc-5-715-2011, 2011. 202

Winkelmann, R., Levermann, A., Martin, M. A., and Frieler, K.: Increased future ice discharge from Antarctica owing to higher snowfall, Nature, 492, 239–242, doi:10.1038/nature11616, 2012. 195

Wolf, D.: The normal modes of a uniform, incompressible Maxwell half-space, J. Geophys. Res. Lett., 56, 106–117, 1985. 197, 198

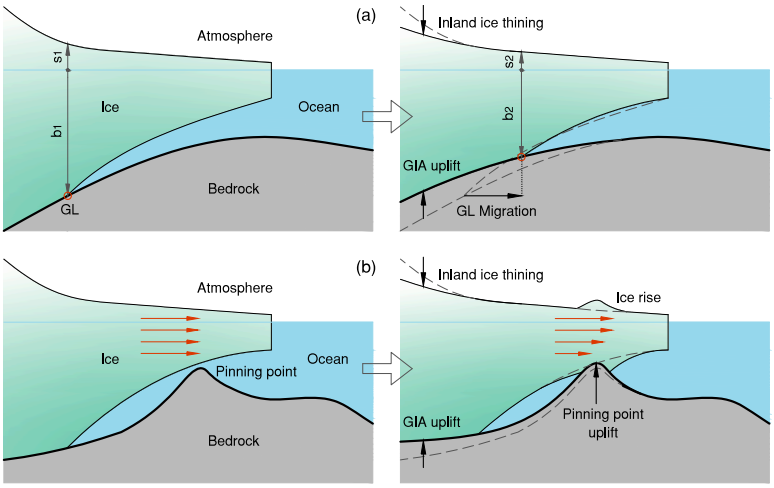

Fig. 1. Schematic of IS/SE feedbacks. **(a)** GL migration controlled by the local sea depth. For equilibrium sea level, the GIA uplift due to thinning of the inland ice promotes the GL migration towards the continental shelf. The hydrostatic equilibrium requires that $s_1/b_1 = s_2/b_2 = -(\rho_w - \rho)/\rho$, where s_i and b_i are the surface and bedrock elevations (subscript $i = 1,2$ represents the initial and final configurations, respectively), and ρ_w and ρ are the water and ice densities (cf. Eq. 2). **(b)** Pinning point, raised by GIA uplift due to thinning of the inland ice, provides basal resistance and buttressing to the ice sheet. Red arrows depict the velocity profiles. Dashed lines in the final configurations (second column) represent the initial geometry. Note that the destabilizing effects of GIA during the periods of inland ice thickening that causes the bedrock to subside can be conceptualized by reverting the direction of mid-arrows.

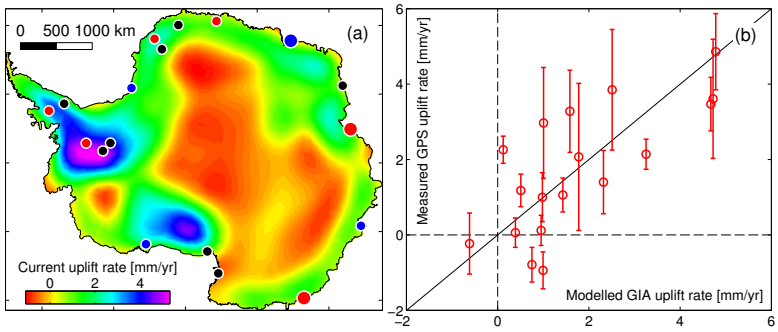

Fig. 2. Model tuning and predictions of current uplift rate. **(a)** Modeled GIA uplift rate at present-day. Calculations are made by forcing the ISSM/GIA model by ice loading history over the past 21 kyr (Supplement Fig. S2) (Ivins et al., 2013). Black circles locate the position where model results are within 1-σ uncertainty range of GPS measurements (Fig. 2b). Red circles represent for cases where model overestimates the measurements, whereas blue circles indicate locations where model underperforms. Big circles are to denote the absolute misfits that are $> 0.75\,\mathrm{mm\,yr^{-1}}$. **(b)** Validation of the model against 18 high-precision GPS uplift data (Thomas et al., 2011). Error bars depict 1-σ uncertainties associated with the GPS measurement.

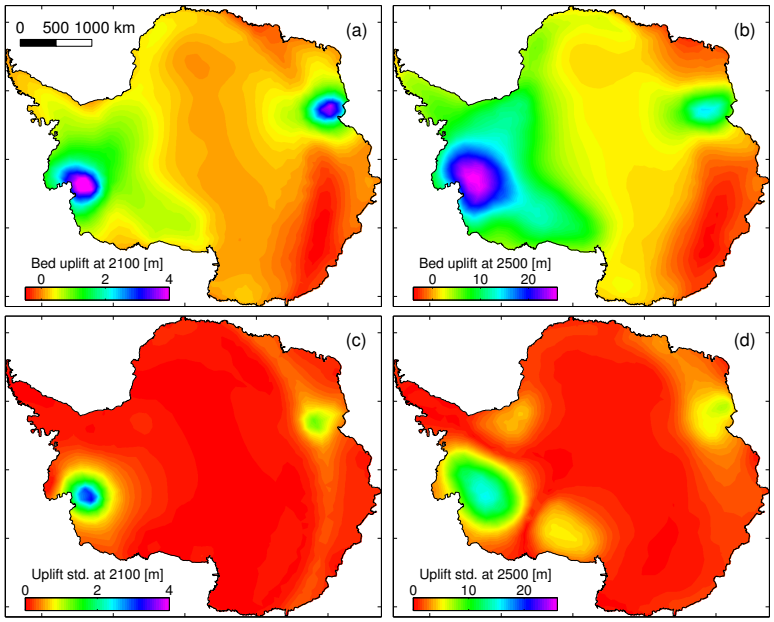

Fig. 3. First-order estimates of the future Antarctic bed uplift. Average model predictions for bed uplift at **(a)** 2100 AD and **(b)** 2500 AD under the proxy RCP 8.5 scenario. Associated standard deviations are shown in subplots **(c)** and **(d)**, respectively. Calculations are made by forcing the calibrated ISSM/GIA model (Fig. 2) by the future ice loadings (Supplement Fig. S3) obtained from the SeaRISE project (Bindschadler et al., 2013; Nowicki et al., 2013). See Supplement Fig. S6 for corresponding solutions for the bed uplift rate. Roughly similar spatial patterns are obtained, with the respective range of values $[-5, 45]$ and $[-10, 70]\,\mathrm{mm\,yr^{-1}}$ at 2100 and 2500 AD.

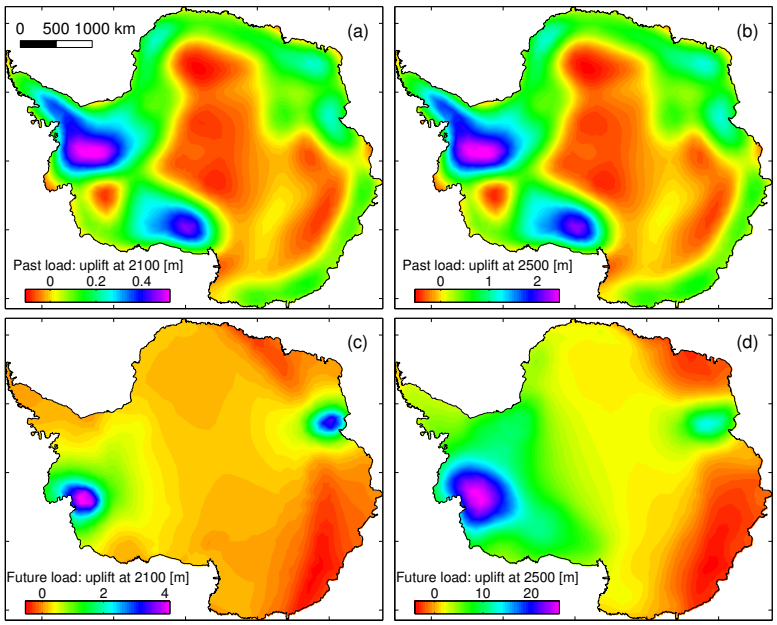

Fig. 4. Role of past and future ice loadings on the future bed topography. GIA uplift at **(a)** 2100 AD and **(b)** 2500 AD obtained by forcing the calibrated ISSM/GIA model (cf. Figure 2.) by the past loading alone. Future DIHs are assumed to be zero. Corresponding solutions (model average) at **(c)** 2100 AD and **(d)** 2500 AD associated with future ice loading alone. Past DIHs are assumed to be zero. Note that we use different color scale in order to illustrate the spatial distributions. See Supplement Fig. S7 where we replot some of these figures with same color scale for ease of comparing magnitudes of uplift.

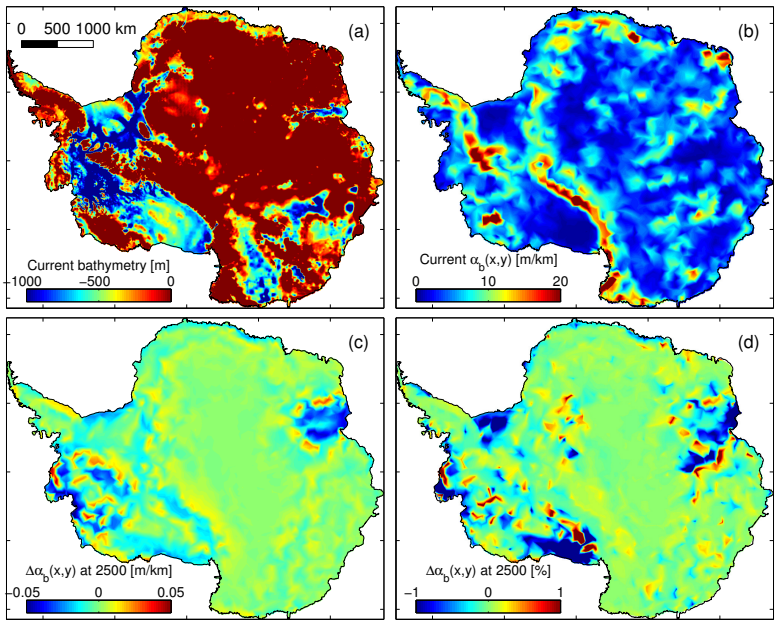

Fig. 5. Estimated change in Antarctic bed slope in future. Present-day **(a)** bathymetry and **(b)** bed slope, $\alpha_b(x,y)$, of Antarctica. To facilitate discussions, only data in the range $[-1000,0]$ m are shown in Fig. 5a. **(c)** And **(d)** model average change in bed slope, $\Delta\alpha_b(x,y)$, at 2500 AD. Negative magnitudes of $\Delta\alpha_b(x,y)$ imply that bedrock will have less steep slopes in the future.

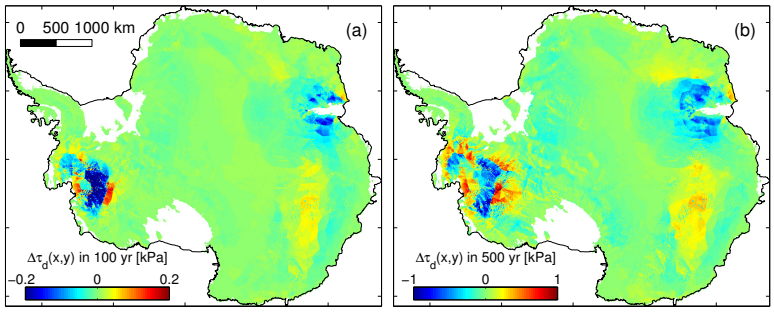

Fig. 6. Influence of GIA uplifts on the gravitational driving stress. Change in driving stress, $\Delta\tau_d(x,y)$, due to the predicted bed uplifts at **(a)** 2100 AD and **(b)** 2500 AD. Calculations are made for the current distribution of ice thickness. Negative magnitudes imply that surface slopes flatten in the future. As the GIA solutions only perturb the ice/bedrock contact area, we mask out the ice shelves in the figures.

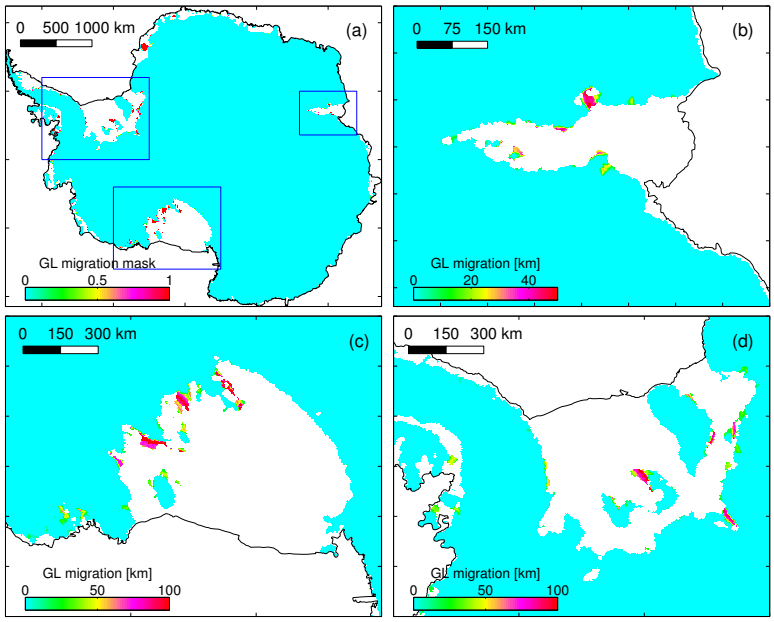

Fig. 7. Influence of GIA uplifts on the GL. **(a)** The mask of GL migration associated with the GIA solutions at 2500 AD. Calculations are based on the hydrostatic equilibrium criterion for the current distribution of ice thickness. Cyan depicts the extent of present-day grounded ice. Red shows the GL advance due to the GIA uplifts. Minor retreats in GL are predicted in a few areas along the Wilkes Land in the EAIS; these are not visible in the figure as their extents are limited to one or two mesh elements, i.e. ≈ 10 km. Blue boxes enclose three important regions that are magnified: **(b)** Amery Ice Shelf, **(c)** Ross Ice Shelf, and **(d)** Ronne Ice Shelf and Bellingshausen Sea Sector. Color codes illustrate the magnitude of GL advance measured along the ice flowlines.

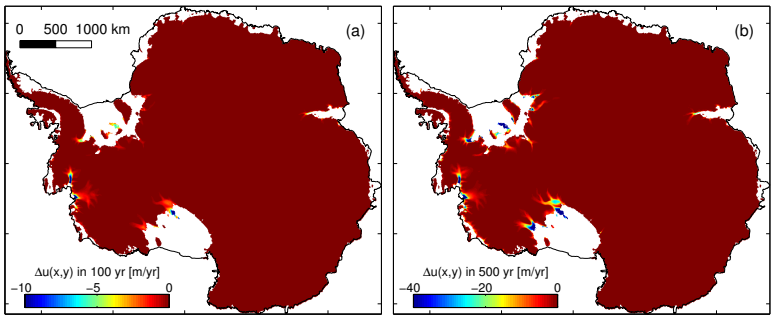

Fig. 8. Influence of GIA uplifts on the ice surface velocities. Change in ice surface velocity, $\Delta u(x,y)$, due to the predicted bed uplifts at **(a)** 2100 AD and **(b)** 2500 AD. Calculations are made by running the diagnostic simulation of 3-D ice flow (higher-order) capability of ISSM. Other model setup and boundary conditions are consistent with those of the SeaRISE control experiment (cf. Bindschadler et al., 2013). A systematic reduction in velocity, which can be attributed partly to the reduction in $\tau_d(x,y)$ (around the Amundsen Sector and Amery Ice Shelf; cf. Fig. 6.) and partly to the GL advance (particularly in the large ice shelves; cf. Fig. 7.), indicates the stabilizing effects of GIA uplift on the future dynamics of AIS.

Discussion Paper | Discussion Paper | Discussion Paper | Discussion Paper |